Optimising the Magnetic Performance of Co Ferrite Nanoparticles via Organic Ligand Capping

M. Vasilakaki[a], N. Ntallis[a], N. Yaacoub[b], G. Muscas[c], D. Peddis[d]*, and K. N. Trohidou[a]**
[a].Institute of Nanoscience and Nanotechnology, NCSR "Demokritos", 153 10 Aghia Paraskevi, Attiki, Greece
[b].Institut des Molécules et Matériaux du Mans (IMMM) - UMR CNRS, Le Mans Cedex, 7 2085, France
[c].Department of Physics and Astronomy, Materials Physics, Uppsala University, Box 516, SE-751 204 Uppsala, Sweden
[d]. Istituto di Struttura della Materia-CNR, 00015 Monterotondo Scalo (RM), Italy

Corresponding Author
*davide.peddis@cnr.it
**k.trohidou@inn.demokritos.gr

1. Exchange ligand process

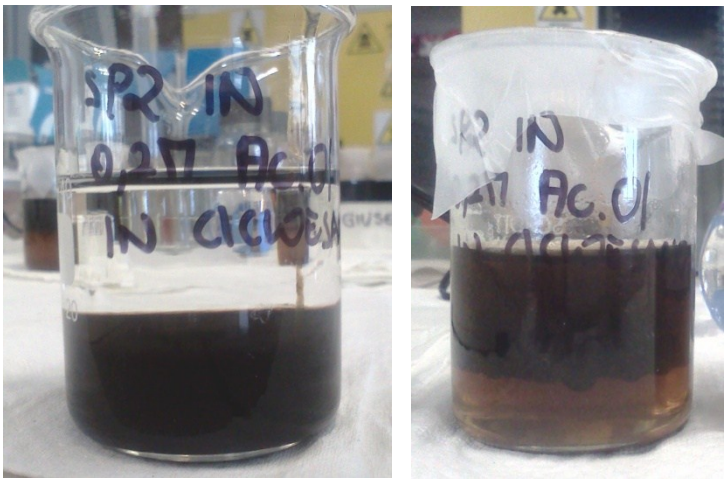

Figure S1. Solution before exchange ligand process (left) and after exchange ligand process (right).

2. Structural and morphological characterisation

X-ray diffraction (XRD) patterns were measured by a Seifert diffractometer with a θ-θ Bragg-Brentano geometry, with Cu-K_α wavelength (1.54056 Å). The samples, in the form of powder, were analysed on a zero-background silicon holder in the 2 θ range 10-80°. The average coherent crystalline domain size was calculated using the Scherrer equation:

$$D_{XRD} = \frac{K\lambda}{\beta \cos \vartheta} \qquad (1)$$

Where K is the shape factor (0.9 for spherical-like particles), λ is the Cu-K_α wavelength, ϑ the Bragg angle, β is the full width at half maximum intensity (FWHM) of the reference peak, after subtracting the instrumental line broadening, determined by measuring a polycrystalline and strain-free sample of Al_2O_3 which has been used as a reference.

The X-ray diffraction (XRD) patterns of the as-synthesised sample (DEG) and the sample after exchange ligand (OA) are reported in Figure S2. All the exhibited Bragg peaks are compatible with the cubic spinel structure of $CoFe_2O_4$ (PDF card 00-22-1086); no other phases are detected. The size of the coherent crystalline domain, determined using equation (1), has been estimated in 5.0(7) nm and 4.5(7) for DEG and OA sample respectively.

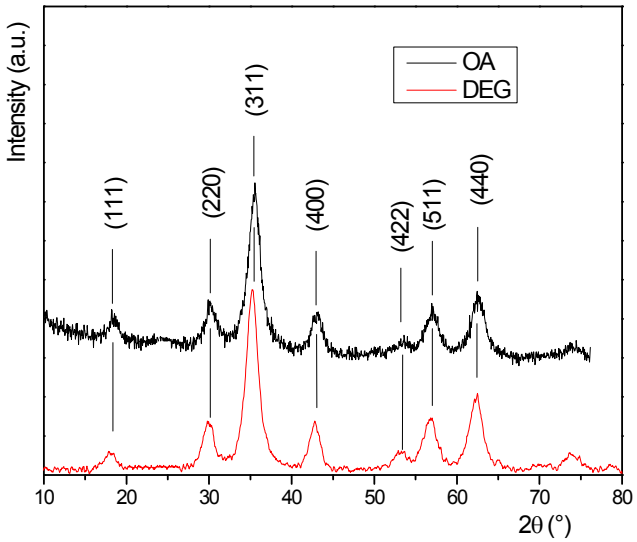

Figure S2. The XRD pattern of the sample as prepared by the polyol process (DEG) and coated by oleic acid (OA). The Bragg's peaks are compatible with the cubic spinel structure of $CoFe_2O_4$ (PDF card 00-22-1086).

For TEM observations, the sample powders were dispersed in isopropyl alcohol and submitted to an ultrasonic bath; then the suspensions were dropped on carbon-coated copper grids and observed using a TEM (FEI Tecnai 12 G2 Twin) equipped with an electron energy filter (GATAN Bio-filter), and a Peltier cooled charge-coupled-device-based slow scan camera (GATAN 794 IF). TEM images were analysed with ImageJ software[1]. The contours of each particle were manually defined, and thanks to the automated measurement suite of the software, the exact particle area has been calculated. Then, assuming a spherical particle shape and knowing the area, the diameter D has been calculated for each particle. Finally, the diameters have been fitted with a log-normal function:

$$P = \frac{A}{D\, w \sqrt{2\pi}} exp - \left[\frac{ln^2\left(D / \langle D_{TEM} \rangle \right)}{2w^2} \right] \qquad (2)$$

where A is the area of the peak, w, the standard deviation of the natural logarithm of the variable D and $<D_{TEM}>$ is the median of the log-normal distribution that gives an estimation of the average particle size.

From the analysis of the TEM images an average particle diameter of 5.3(9) nm has been calculated, compatible with single crystalline particles. The nanoparticles have a spherical-like shape (Figure S3 a-b) and a narrow size distribution (Figure S3 c) with a standard deviation of 0.9 nm.

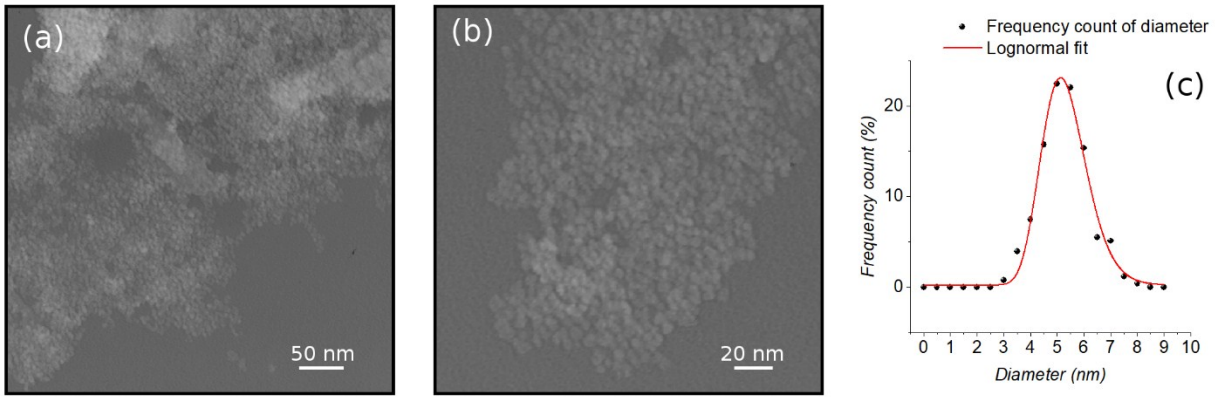

Figure S3. TEM Panels (a) and (b) confirm the homogenous size and shape distribution of the nanoparticles. Panel (c) reports the size calculated distribution with lognormal fit. The *average* particle size is 5.3(9) nm.

3. DFT electronic structure calculations for the magnetic anisotropy

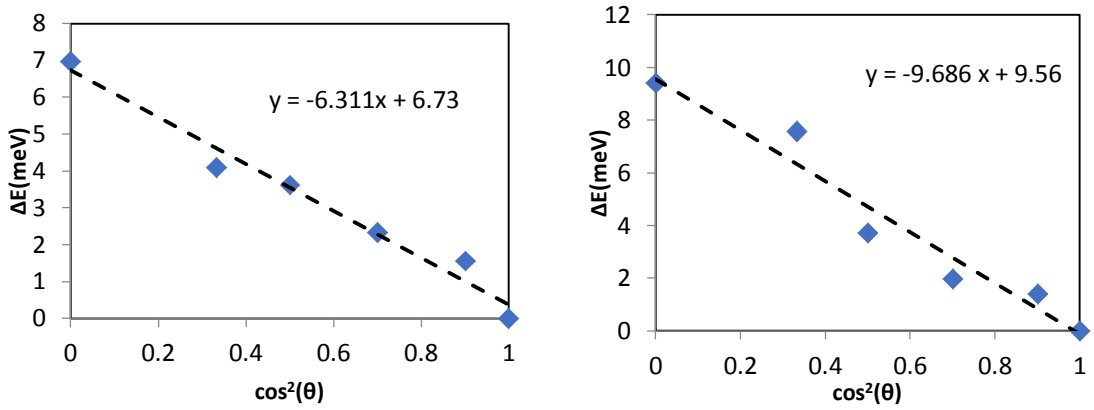

Figure S4. Variation of the energy difference of the a) DEG sample and b) OA sample as a function of the squared cosine of the polar angle. The slope is an estimation of the magnetic anisotropy energy.

4. Distribution of magnetic anisotropy energy

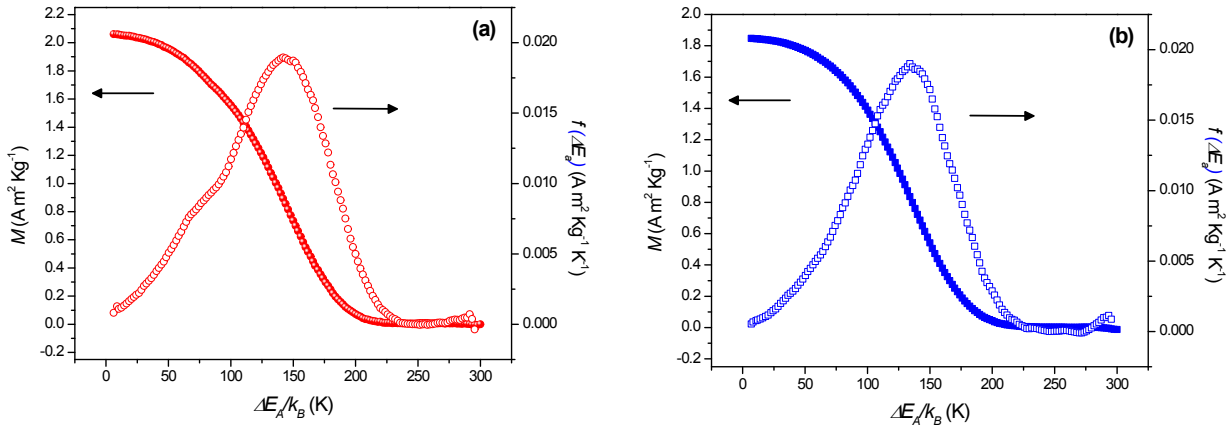

Figure S5. M_{FC}-M_{ZFC} (full symbols) and the corresponding derivative curves (empty symbols) for the DEG (a) and the OA (b) sample, respectively.

For a magnetic nanoparticles' (MNPs) ensemble it can be easily demonstrated that [2]

$$M_{TRM} = M_{FC} - M_{ZFC} + M_{IRM} \qquad (3)$$

Where M_{TRM} and M_{IRM} are the thermoremanent magnetization and the isothermal remanent magnetization respectively. However, as M_{IRM} is negligible in the NPs assemble, $M_{FC} - M_{ZFC}$ can be considered as a very good approximation of M_{TRM} [2–5]. For both samples $M_{FC} - M_{ZFC}$ shows (Figure S5) a decrease with increasing temperature, as it is expected for an assembly of magnetic monodomain particles. For non-interacting particles, the derivative of this curve gives an estimate of the anisotropy energy barrier distribution[6,7] :

$$f(\Delta E_A) \propto -\frac{dM_{FC-ZFC}}{dT} \qquad (4)$$

Due to the presence of interparticle interactions in our samples, the derivative of M_{FC-ZFC} (Figure S5) can actually be considered only as a rough estimation of the E_A distribution, including the effect of the interparticle interactions themselves. Within the Néel model, the blocking temperature can be defined as the temperature for which the relaxation time is equal to the measuring time of the experimental technique. In a real system of nanoparticles, where a finite size distribution always exists, T_b is often defined as the temperature at which 50% of the sample is in the superparamagnetic state[8]. Since T_b is proportional to E_A, an estimate of the T_b distribution can be obtained from the E_A distribution by evaluating the temperature at which 50% of the particles overcome their anisotropy energy barriers. Values of T_b are reported in Table 3 in the main text.

5. Comparison of the 3-spin with the SW model

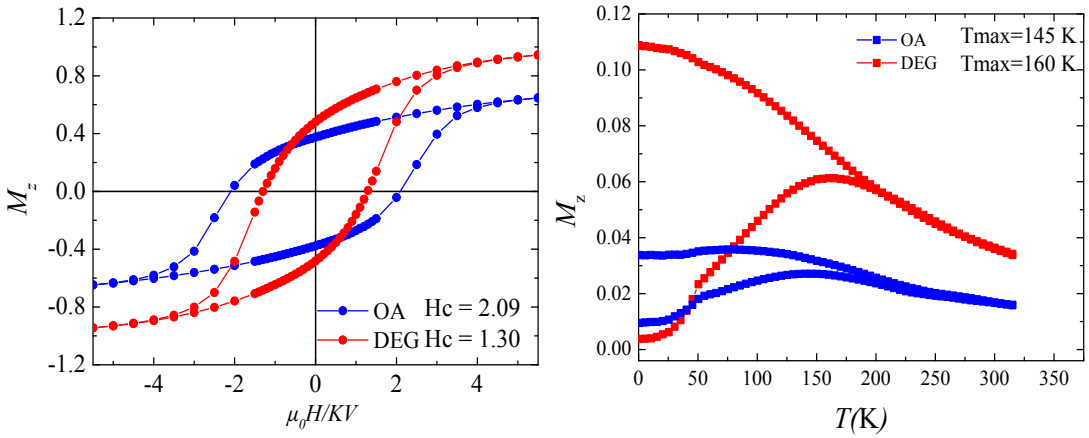

Figure S6. Monte Carlo simulation results for the hysteresis loops (left) and the ZFC/FC magnetisation curves (right) for the $CoFe_2O_4$ nanoparticles coated with DEG (red) and OA (blue), using the single spin mesoscopic approach for the two nanoparticle assemblies.

6. Interparticle Interactions: measurements and calculation of the IRM and DCD plots

DEG sample OA sample

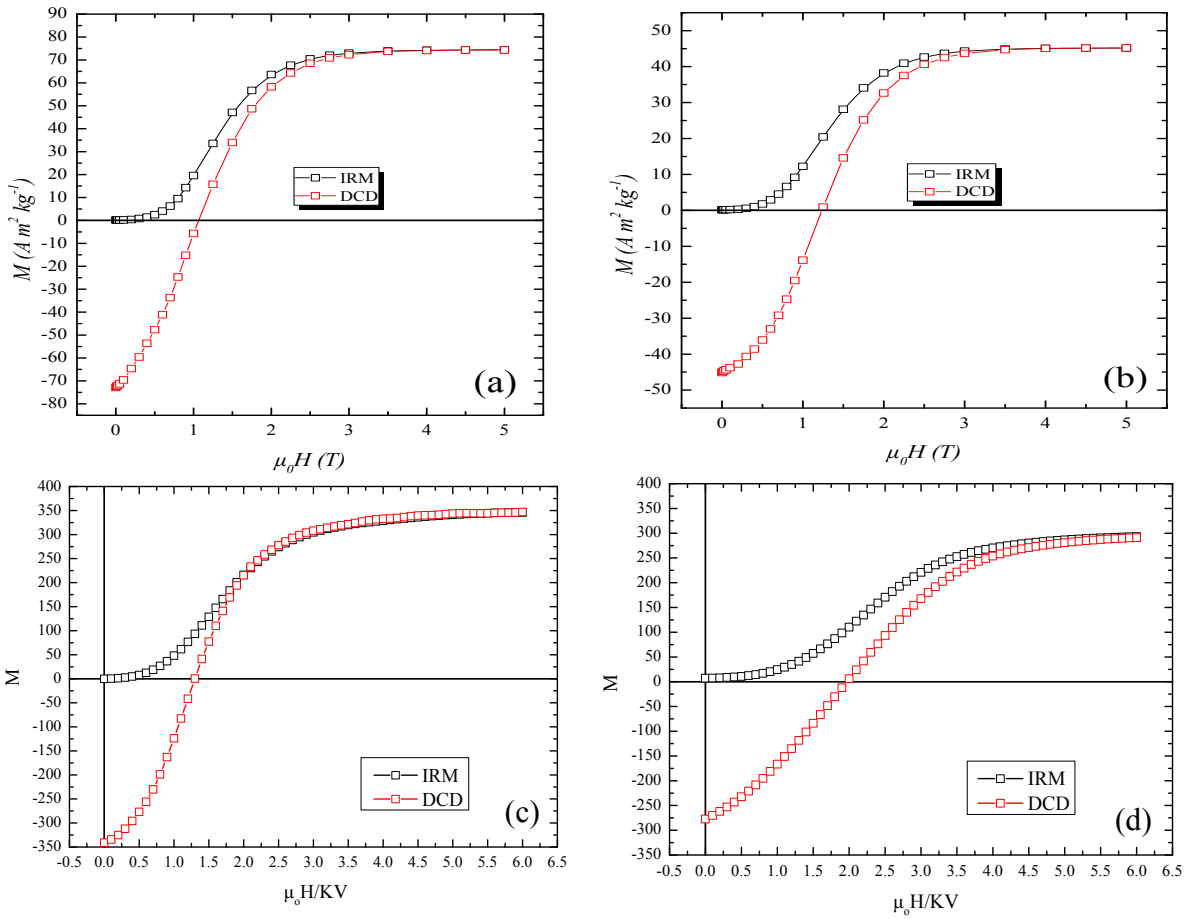

Figure S7. Isothermal Remanent Magnetization (IRM) (black) and Direct Current Demagnetization (DCD) (red) remanent curves recorded at 5 K for the DEG (a) and OA (b) samples together with the MC simulation results of IRM and DCD magnetization curves of an assembly of interacting $CoFe_2O_4$ nanoparticles coated with DEG (c) and OA (d) surfactants.

The analysis of remnant magnetization curves measured by IRM and DCD protocols allowed also to investigate the interaction regime among particles. For an assembly of non- interacting single-domain particles with uniaxial anisotropy and with coherent magnetization reversal the two remanence curves are related via the Wohlfarth equation [9]

$$m_{DCD}(H) = 1 - 2m_{IRM}(H) \quad (5)$$

where $m_{DCD}(H)$ and $m_{IRM}(H)$ represent the reduced terms $M_{DCD}(H)/M_{DCD}(5T)$ and $M_{IRM}(H)/M_{IRM}(5T)$ and $M_{DCD}(5T)$ and $M_{IRM}(5T)$ are the remanence values for the DCD and IRM curves at 5 T, respectively.

Kelly et al.[10] rewrote the Wohlfarth relation (eq 5) to explicitly reveal deviations from a noninteracting case:

$$\Delta M = M_{DCD} - (1 - 2M_{IRM}) \quad (6)$$

In particular, a negative deviation from the linearity is an evidence of the predominance of dipole−dipole interactions, while a positive deviation can be attributed to the predominance of exchange interactions.

In our case, the different molecular coating changes not only magnetic features but also interparticle distance. In the OA sample for each particle a ~2 nm thickness of oleic acid produces a total of ~4 nm of distances among surfaces. On the other hand, the side chain link of the short chain DEG, produces a single layer of 0.5 nm with a total distance of 1 nm among particles' surfaces. The above lengths of the OA and the DEG molecules are rough estimations obtained by a simple calculation starting from density and surface area for 1 g monolayer.[11,12]

The influence of particles' distance on the dipolar interaction energy is roughly described by the relation :

$$E_{dip} \approx \frac{\mu_0 \mu^2}{4\pi d^3} \qquad (7)$$

Clearly, from eq. (7) a difference is expected between the two samples. The analysis of ΔM-plots (Figure 7) evidences negative deviation in both curves (sign of the prevalence of dipolar interactions). This deviation is proportional to the intensity of interparticle interaction energy. The intensity of the negative deviation is more than two times larger for the DEG sample, though the reversal field for both samples is similar (around ≈ 0.85 T). This 2.5 ratio of the deviation for the two samples is in agreement with the estimated ratio of their dipolar interaction energies (~ 31 K and ~12 K for DEG and OA respectively, as they are given by eq. (7)). This is expected since the larger interparticle distance produced by the oleic acid coating, results to weaker interparticle interactions for this sample.

7. Effect of the concentration of the particles on the magnetic properties

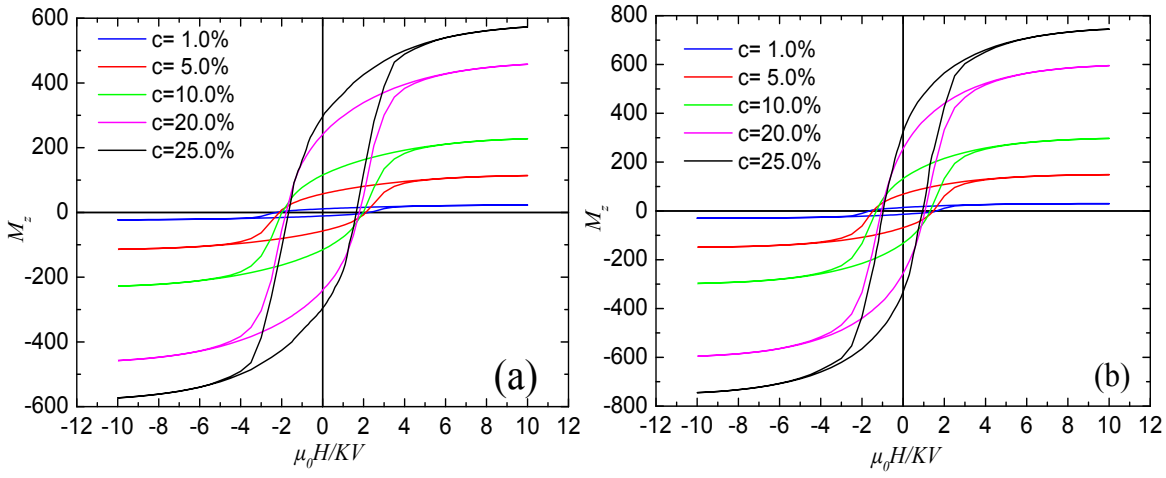

Figure S8. Monte Carlo hysteresis loops of the $CoFe_2O_4$ nanoparticles coated with OA (a) and DEG (b), sample for various concentrations of the nanoparticles.

References

[1] C. A. Schneider, W. S. Rasband, K. W. Eliceiri, *Nat Meth* 2012, **9**, 671.

[2] R. W. Chantrell, M. El-Hilo, K. O'Grady, *IEEE Trans. Magn.* 1991, **27**, 3570.

[3] L. Del Bianco, D. Fiorani, A. Testa, E. Bonetti, L. Signorini, *Phys. Rev. B* 2004, **70**, 052401.

[4] A. Scano, V. Cabras, F. Marongiu, D. Peddis, M. Pilloni, *Mater. Res. Express* 2017, **4**, 025004.

[5] D. Peddis, M. T. Qureshi, S. H. Baker, C. Binns, M. Roy, S. Laureti, D. Fiorani, P. Nordblad, R. Mathieu, *Philos. Mag.* 2015, **6435**, 1.

[6] C. Cannas, A. Musinu, G. Piccaluga, D. Fiorani, D. Peddis, H. K. Rasmussen, S. Mørup, *J. Chem. Phys.* 2006, **125**, 164714.

[7] D. Peddis, M. V Mansilla, S. Mørup, C. Cannas, A. Musinu, G. Piccaluga, F. D. Orazio, F. Lucari, D. Fiorani, *J. Phys. Chem. B* 2008, **112**, 8507.

[8] D. Peddis, C. Cannas, A. Musinu, A. Ardu, F. Orru, D. Fiorani, S. Laureti, D. Rinaldi, G. Muscas, G. Concas, G. Piccaluga, *Chem. Mater.* 2013, **25**, 2005.

[9] E. P. Wohlfarth, *J. Appl. Phys*., 1958, **29**, 595–596.

[10] P. E. Kelly, K. O. Grady, P. I. Mayo and R. W. Chantrell, *IEEE Trans. Magn*., 1989, **25** 3881–3883.

[11] A. G. Roca, M. P. Morales, K. O'Grady, C. J. Serna, *Nanotechnology* 2006, **17**, 2783.

[12] D. Peddis, F. Orrù, A. Ardu, C. Cannas, A. Musinu, G. Piccaluga, *Chem. Mater.* 2012, **24**,

1062.